Journal of Materials Chemistry A

Accepted Manuscript

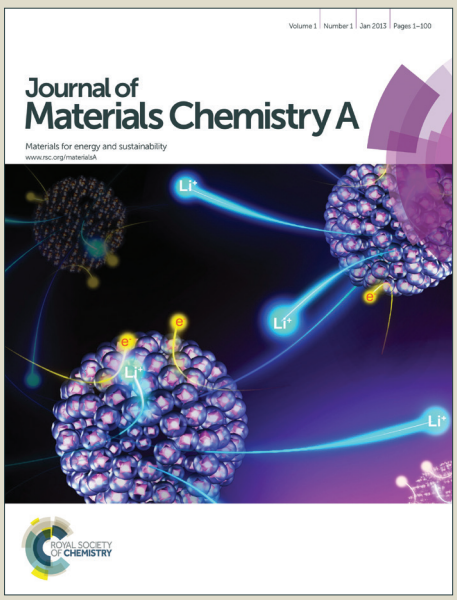

ROYAL SOCIETY OF CHEMISTRY

www.rsc.org/materialsA

Cite this: DOI: 10.1039/c0xx00000x

www.rsc.org/xxxxxx

ARTICLE TYPE

$Ni_{0.31}Co_{0.69}S_2$ Nanoparticles Uniformly Anchored on the Porous Reduced Graphene Oxide Framework for High Performance Non-enzymatic Glucose Sensor

Guilin Li, Huanhuan Huo, Cailing Xu*

Received (in XXX, XXX) Xth XXXXXXXXX 200X, Accepted Xth XXXXXXXXX 200X
DOI: 10.1039/b000000x

The $Ni_{0.31}Co_{0.69}S_2$ nanoparticle/reduced graphene oxide ($Ni_{0.31}Co_{0.69}S_2$/rGO) composites have been synthesized via hydrothermal method and then applied as the active materials for high performance non-enzymatic glucose sensor. Field emission scanning electron microscopy (FESEM) and transmission electron microscopy (TEM) were employed to characterize the morphology of the as-prepared samples. The results revealed that the abundant nanoparticles with the size of about 150 nm uniformly anchored on the reduced graphene oxide nanosheets which are interconnected to form porous graphene framework. The subsequent electrochemical measurements and kinetic analysis showed that the $Ni_{0.33}Co_{0.67}S_2$/rGO composites possessed the excellent electrocatalytic activity to glucose oxidation with a low detection limit of 0.078 μM and wide linear range of 0.001-5 mM and 5-16 mM. And the sensitivities for two liner ranges are 1753 μA mM^{-1} cm^{-2} and 954.7 μA mM^{-1} cm^{-2}, respectively. Additionally, the favorable selectivity, long-term stability and superior practical application were also obtained. All these results indicate the $Ni_{0.33}Co_{0.67}S_2$/rGO composites are a promising active material for non-enzymatic glucose sensors.

1. Introductionμ

The increasing demands of fast and reliable determination of glucose in the areas of clinical diagnostics, food industry and biotechnology have attracted tremendous efforts to develop a glucose sensor with high sensitivity, excellent selectivity and good reliability.[1, 2] Non-enzymatic glucose sensors based on the direct electrocatalytic oxidation of glucose on the electrode have triggered great interest and been widely investigated due to its high sensitivity, long-term stability, fast response time and simple operation.[3, 4] So far, noble metals and their alloys, transition metal and their oxides or hydroxides are conventional electrode materials for non-enzymatic glucose sensors.[5-10] But their applications are restricted by their high cost, low antitoxic ability, poor operational stability or limited electronic conductivity.[3] Thus, the development of newly advanced electrode materials with high performance for glucose sensors is essential.

Recently, transition metal sulfides have been subject to intense research as new functional materials due to their excellent intrinsic properties and good electrochemical performance.[11] They have been widely used in many fields such as supercapacitors, hydrogenation catalysts, dye-sensitized solar cells and lithium ion batteries and so on.[12-15] Very recently, transition metal sulfides (such as Cu_xS, Ni_xS) have been directly used as electrode materials for glucose sensors and received some attention. For example, Yang *et al.*[16] reported that the flower-like CuS nanoparticles have exhibited a sensitivity of 5.86 μA mM^{-1} and a linear range of 0.01-10 mM for non-enzymatic glucose detection. Cu_2S nanoplates synthesized by Swarup Kumar Maji *et al.* showed the sensitivity of 61.67 μA mM^{-1} and linear range of 0.01-3.1 mM towards glucose determination.[17] Lin *et al.*[18] have prepared Ni_3S_2/MWCNT composites onto Ni foam for non-enzymatic glucose detection. This composite exhibited a high sensitivity up to 3345 μA $mM^{-1}cm^{-2}$, but the performance was compromised due to the narrow linear range of 0.03-0.5 mM and the high applied potential of 0.54 V (vs Ag/AgCl). Besides, our group has also synthesized 3D Ni_3S_2 nanosheet arrays directly grown on Ni foam by hydrothermal method for glucose oxidation and achieved a high sensitivity of 6148 μA $mM^{-1}cm^{-2}$ at 0.55 V(vs Hg/HgO) and the linear range of 0.005-3.0 mM.[19] Even so, the present research in this field is still in its infancy and a little

data are available. This can be considered as limited successes because of the unbalanced electrocatalytic performance such as low sensitivity, narrow linear range or high applied potential.[4] Thus, it is quite necessary for further study to explore and develop the electrode materials of transition metal sulfides by effective routes in order to achieve high performance glucose sensors.

According to the previous reports about glucose sensors, the stability, conductivity, oxidation potential and specific surface area of nanostructured materials are the key impacts for electrochemical performance of sensors.[3, 20] Thus, two feasible methods can be developed to improve the electrocatalytic properties of active materials, including designing bimetallic Ni-Co sulfide materials and preparing graphene-based composites. On one hand, Ni-Co bimetallic nanomaterials which incorporate cobalt into the Ni-based materials will deliver superior electrochemical properties compared to the corresponding monometallic counterparts, such as the lower redox potentials, the enhanced stability and the increased electroactive sites due to the possible valence interchange or charge hopping between Co and Ni cations.[7, 21-24] On the other hand, graphene have been considered as an excellent supporting matrix for nanostructured catalysts due to the advantages of high surface area and excellent conductivity.[25-28] For example, NiO/GM (graphene macroassembly) hybrid modified electrode synthesized by Liu *et al.* has exhibited a high sensitivity of 918 μA $mM^{-1}cm^{-2}$ and a linear range of 1-100μM, which is superior to NiO nanosphere modified electrode reported previously.[29] Furthermore, Zhan et al.[30] fabricated $Ni(OH)_2$/3D graphene foam as a electrochemical electrode for non-enzymatic glucose detection. The electrode exhibits remarkable electrocatalytic activity of a high sensitivity (2.65 mA $mM^{-1}cm^{-2}$), low detection limit (0.34 mM) and a linear response from 1 μM to 1.17 mM to glucose oxidition.

Inspired by the advantages of bimetallic Ni-Co sulfide materials and graphene-based composites, the $Ni_{0.31}Co_{0.69}S_2$/rGO composite material was synthesized via a hydrothermal method and firstly used as the active material for non-enzymatic glucose sensor in this present work. The electrochemical characterization showed that this material exhibited an excellent electrochemical performance because of the unique nanostructure and excellent electrocatalytic activity of bimetallic $Ni_{0.31}Co_{0.69}S_2$. Furthermore, the kinetic analysis indicated that the $Ni_{0.31}Co_{0.69}S_2$/rGO composites have low charge transfer resistance, large diffusion coefficient (D) and catalytic rate constants (K_{cat}) for glucose oxidation. Therefore, the $Ni_{0.31}Co_{0.69}S_2$/rGO composite is promising for the application of non-enzymatic glucose sensors.

2. Experimental section

2.1 Materials

$NiCl_2·6H_2O$, $CoCl_2·6H_2O$ and other reagents in this experiment were of analytical purity and used as received without further purification. Ultrapure water (18.2 MΩ cm^{-1}) generated by an Aike water system was used throughout the work.

2.2 Synthesis of GO and rGO samples.

Graphene oxide (GO) was first prepared from natural graphite (15000 mesh) by the modified Hummers' method[31, 32]. And then GO was dispersed in ultrapure water to form a 2 mg ml^{-1} homogeneous suspension after 1 h ultrasonication. The zeta potential of the GO suspension is -29.3mV, demonstrating the well dispersibility of the as-prepared GO sheets in water.

6ml as-prepared GO suspension was transferred into a weighting bottle (25×40). Subsequently, the weighting bottle was loaded into a Teflon-lined stainless steel autoclave and the autoclave was maintained at 180 ℃ for 10 h. After freeze-dried for 24 h in freeze dryer, reduced graphene oxide (rGO) was obtained.

2.3 Synthesis of $Ni_{0.31}Co_{0.69}S_2$/rGO composite.

The $Ni_{0.31}Co_{0.69}S_2$/rGO composite was prepared according to the following procedure: 26.7 mg $NiCl_2·6H_2O$ and 53.5 mg $CoCl_2·6H_2O$ (the content of Co^{2+} is 67%) were dissolved in 6 mL as-prepared GO suspension by magnetic stirring and ultrasonication for 10min, respectively. Then, 256.8 mg thiourea was introduced into the above suspension, followed by magnetic stirring and ultrasonication for 20 min, respectively. Subsequently, the mixture was transferred into a weighting bottle and loaded into a Teflon-lined stainless steel autoclave. And the autoclave was maintained at 180 ℃ for 10 h. After cooling to room temperature, a hydrogel product (diameter of 1.5cm and high of 1.2cm) was obtained. It was taken out and immersed into water overnight to remove the remaining ions. Finally, the product was freeze-dried for 24 h in freeze dryer.

For comparison, a series of samples were synthesized under the same condition by keeping the Co^{2+} content in initial solutions at 0%, 50%, 74% and 100%.

2.4 Material characterization

The morphology of $Ni_{0.31}Co_{0.69}S_2$/rGO composites were characterized by field emission scanning electron microscopy (FESEM, JEOL JSM-S4800) and transmission electron microscopy (TEM, TecnaiTM G2F30 with energy dispersive spectroscopy (EDS)). For TEM observation, the freeze-dried samples were suspended in water and then supported on carbon-coated copper grid. Raman spectra were recorded on inVia Raman microscopy system with a laser wavelength of 628 nm. X-Ray diffraction (XRD) data was collected on a Rigaku D/M ax-2400. The Ni/Co molar ratio in the as-prepared samples was obtained by inductively coupled plasma–atomic emission spectroscopy (ICP-AES) using an IRIS Advantage ER/S spectrophotometer. Zeta potentials was recorded on Zeta Potential Report (Zetasizer Nano 3600).

2.5 Fabrication of the working electrode

Firstly, the different freeze-dried composites were ultrasonically dispersed in deionized water in the presence of 0.5 mg mL^{-1} hexadecyltrimethyl ammonium bromide (CTAB) for 2 mg mL^{-1} suspension, respectively. Here, CTAB is just used for increasing the dispersion of the composites in deionized water. The zeta potential (21.6mV) of the suspension prepared using $Ni_{0.31}Co_{0.69}S_2$/rGO composite indicated the advantages of CTAB. Secondly, the glassy carbon electrode (GCE, diameter of 3 mm) was polished with alumina powder and then washed ultrasonically in distilled water and ethanol for a few minutes. After that, 15 μL $Ni_{0.31}Co_{0.69}S_2$/rGO suspension and 2 μL Nafion solution (0.5 wt%) were successively dropped on the pre-treated GCE and dried at room temperature.

2.6 Electrochemical characterization

The electrochemical experiments were performed on a CHI760E electrochemical workstation using a three-electrode system at room temperature: platinum plate as the auxiliary electrode, Ag/AgCl electrode as the reference electrode, the composite modified GCE as the working electrode and 0.3 M NaOH aqueous solution as electrolyte.

In addition, the effects of different pH values (0.1, 0.2, 0.3, 0.5M NaOH) and temperatures (25, 30, 40, 50, 60, 70□) for the electrocatalytic performance of the $Ni_{0.31}Co_{0.69}S_2$/rGO modified GCE were also investigated by amperomteric response.

The detection limit (LOD) is calculated according to the equation as follows[29, 30]:

$$LOD = 3S / N \quad (1)$$

where S is the standard deviation calculated from the current response of seven parallel additions of low glucose concentration solution into the electrolyte; N is the sensitivity of the modified electrode; the number 3 stands for a signal-to-noise ratio.

3. Results and Discussions

3.1 Electrocatalytic performance of different modified electrodes

The ICP results of the as-prepared bimetallic samples indicated that the contents of Co element (45%, 69 and 74%) are close to the values (50%, 67%and 75%) in the initial solutions. Therefore, a series of samples (denoted as NiS_2/rGO, $Ni_{0.55}Co_{0.45}S_2$/rGO, $Ni_{0.31}Co_{0.69}S_2$/rGO, $Ni_{0.26}Co_{0.74}S_2$/rGO and CoS_2/rGO) can be obtained by keeping the Co^{2+} content in the initial solutions.

The electrocatalytic performance of different modified electrodes (NiS_2/rGO, $Ni_{0.55}Co_{0.45}S_2$/rGO, $Ni_{0.31}Co_{0.69}S_2$/rGO, $Ni_{0.26}Co_{0.74}S_2$/rGO and CoS_2/rGO) was firstly investigated by CV measurements for giving the highest sensing performance. As can be seen from Fig.S1A-E, upon the doping of Co, the redox peak gradually shifts to the low potential due to the lower redox potential of CoS_2/CoS_2OH couple. Furthermore, the corresponding catalytic currents of different modified electrodes at different potential were shown in Fig.S1F. It can be seen that the $Ni_{0.31}Co_{0.69}S_2$/rGO modified electrode shows the highest catalytic current at a low potential, demonstrating its excellent electrocatalytic activity for glucose oxidation. The results proved that an appropriate Ni/Co molar ratio is an important factor for high performance electrocatalyst.[7, 33, 34]

3.2 Characterization of the $Ni_{0.31}Co_{0.69}S_2$/rGO sample

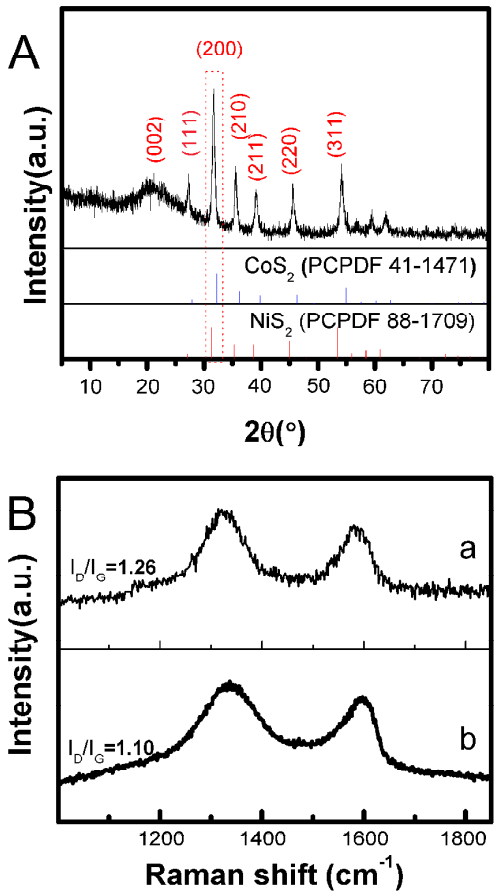

Fig.1 (A) XRD pattern of the $Ni_{0.31}Co_{0.69}S_2$/rGO sample. (B) Raman spectra of the $Ni_{0.31}Co_{0.69}S_2$/rGO (a) and rGO (b) samples.

The typical XRD pattern of the $Ni_{0.31}Co_{0.69}S_2$/rGO sample is shown in Fig.1A. As can be seen, the diffraction peaks at 27.2°, 31.7°, 35.6°, 39.2°, 45.6° and 54.1°, which can be assigned to the (111), (200), (210), (211), (220), (311) planes, are located between the characteristic diffraction peaks of cubic CoS_2 (PCPDF 41-1471) and NiS_2 (PCPDF 88-1709), indicating the atomic scale mixing of Ni and Co ions in the disulphide matrix of the sample.[21] The content of Co, Ni and S element in the EDS pattern (Fig.S2) further demonstrated that it is a bimetallic Ni-Co sulfide. The broad peak at 23° is the (002) plane of reduced graphene oxide.

Raman spectrum was used to characterize the structure and electronic properties of graphene. As shown in Fig.1B, for the $Ni_{0.31}Co_{0.69}S_2$/rGO and rGO samples, two typical peaks around 1350 and 1580 cm^{-1} are ascribed to the disorder (D) and graphite (G) bands of graphene nanosheets. Generally, the I_D /I_G intensity ratio was used to estimate the degree of disorder and average size of the sp^2 domains.[35, 36] The value of I_D:I_G for the $Ni_{0.31}Co_{0.69}S_2$/rGO sample (1.26) is higher than that of rGO (1.10), implying the existence of more defects/disorders or decreased sp^2 domains in the graphene nanosheets. This can be attributed to the anchor of nanoparticle on the graphene nanosheets. Furthermore, the slightly red shifted D and G bands of the $Ni_{0.31}Co_{0.69}S_2$/rGO sample revealed the charge transfer between graphene nanosheets and $Ni_{0.31}Co_{0.69}S_2$ nanoparticles.[37] This can be attributed to the interaction between $Ni_{0.31}Co_{0.69}S_2$ nanoparticles and graphene nanosheets. In addition, the 2D/G intensity ratio has been widely used as a characteristic feature for the number layers in graphene sheets. As shown in Fig. S3, the low $I_{2D}/_{IG}$ values of GO and rGO indicated that both of them contain multilayer of graphene.[38, 39]

Cite this: DOI: 10.1039/c0xx00000x

www.rsc.org/xxxxxx

ARTICLE TYPE

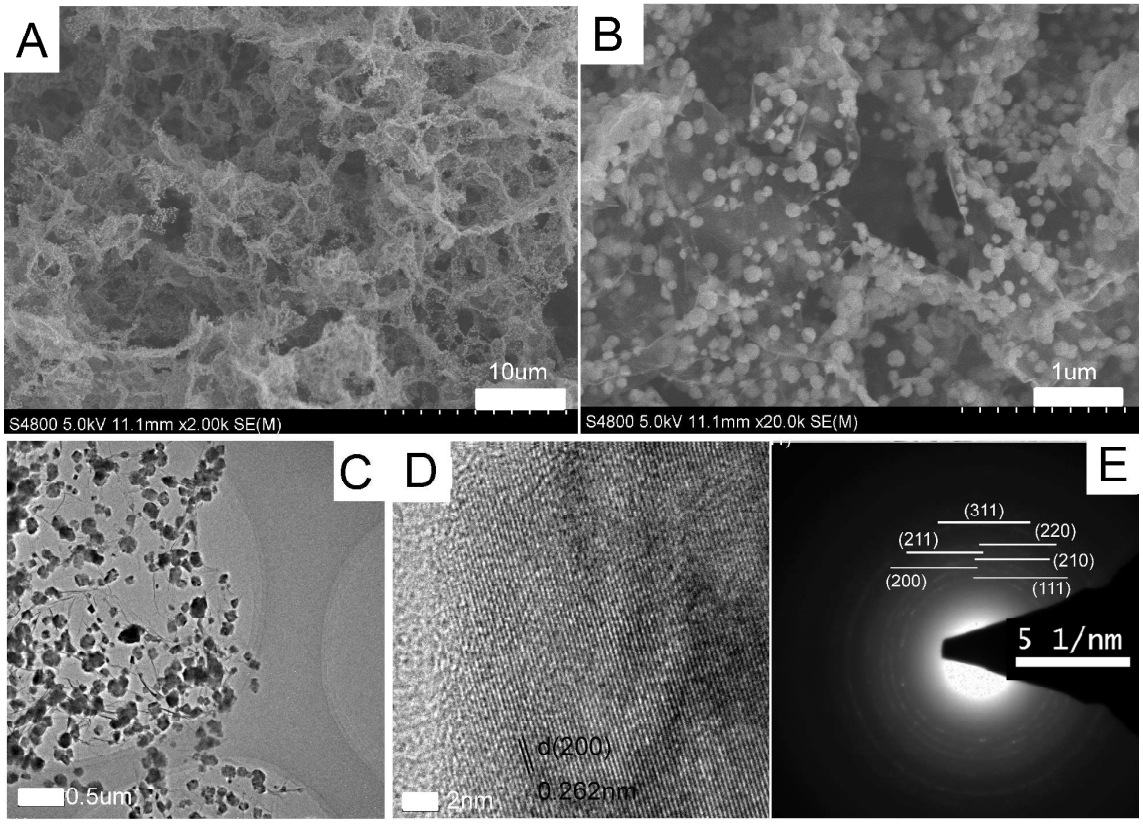

Fig. 2 (A, B) FESEM images, (C) TEM image, (D) HRTEM image and (E) SAED pattern of the $Ni_{0.31}Co_{0.69}S_2$/rGO sample.

The FESEM images (Fig.2A, B) reveal that a great deal of $Ni_{0.31}Co_{0.69}S_2$ nanoparticles uniformly anchored on the interconnected porous graphene framework with pore size from submicrometer to several micrometers. Furthermore, the $Ni_{0.31}Co_{0.69}S_2$ nanoparticles resided on or were encapsulated by the ultrathin graphene nanosheets, resulting in the large contact area between the nanoparticles and high conductive graphene. Such porous graphene framework is beneficial to enhance the transmission rate of ion and electron in electrochemical reaction process. [40]

TEM image (Fig.2C) further defines that the diameter of nanoparticles is about 150 nm, which uniformly located on the ultrathin graphene nanosheets. Additionally, considering the ultrasonication treated before TEM characterization, the absence of isolated nanoparticles demonstrates the strong interaction between $Ni_{0.31}Co_{0.69}S_2$ nanoparticles and graphene nanosheets. The lattice spacing of about 0.262 nm corresponds to the (200) lattice plane of $Ni_{0.33}Co_{0.67}S_2$ crystal, as seen from HRTEM image of Fig.2D. Besides, the SAED pattern of the $Ni_{0.31}Co_{0.69}S_2$/rGO sample (Fig.2E) shows that the multi-layer diffraction rings stands for the polycrystalline features and can be assigned to the (111), (200), (210), (211), (220) and (311) planes (from interior to exterior) of $Ni_{0.33}Co_{0.67}S_2$, which are well consistent with the XRD data.

3.3 Electrochemical performance of the $Ni_{0.31}Co_{0.69}S_2$/rGO modified electrode for glucose detection

Cite this: DOI: 10.1039/c0xx00000x

www.rsc.org/xxxxxx

ARTICLE TYPE

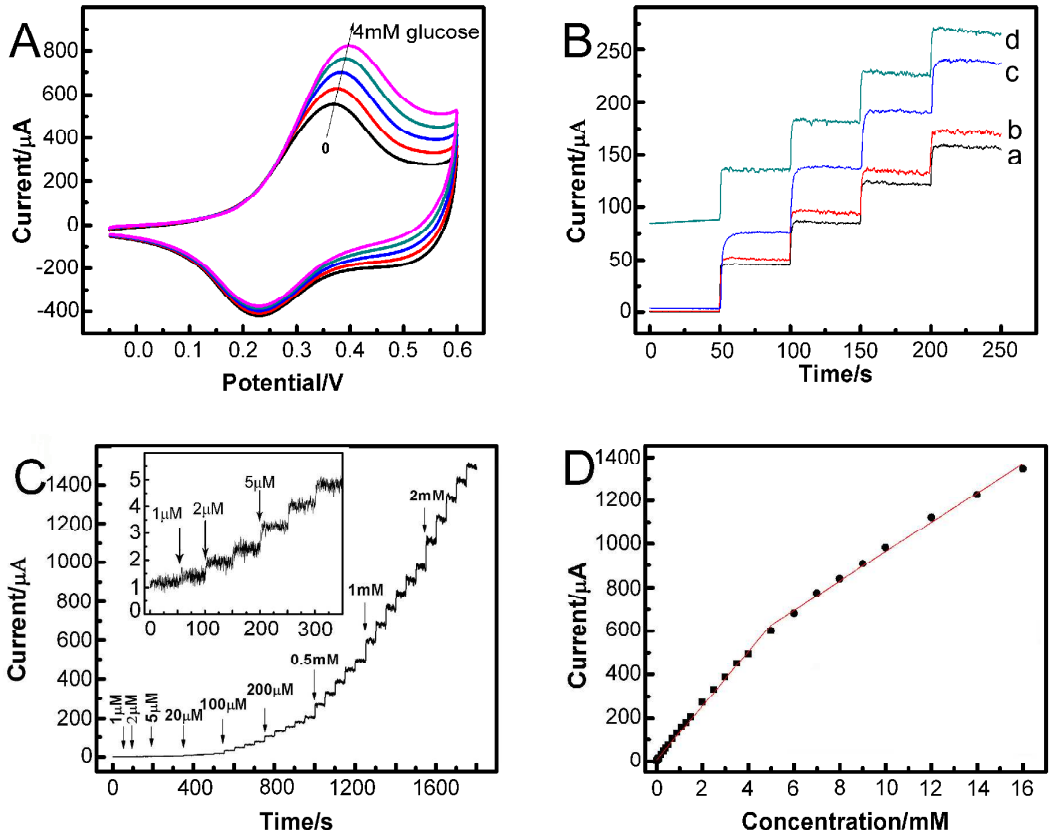

Fig. 3 (A) CVs of the $Ni_{0.31}Co_{0.69}S_2$/rGO modified electrode at 20 mV/s in 0.3 M NaOH solution with different concentration of glucose (from inner to outer curve: 0, 1, 2, 3, 4 mM). (B) Amperometric response of the $Ni_{0.31}Co_{0.69}S_2$/rGO modified electrode at different potentials with successive additions of 0.5 mM glucose (a: 0.4 V, b: 0.45 V, c: 0.5 V and d: 0.55 V vs Ag/AgCl); (C) Amperometric response of the $Ni_{0.31}Co_{0.69}S_2$/rGO modified electrode to successive additions of different concentration glucose solution up to 16 mM (Inset: a partial magnification of the current response toward the low concentration glucose solution.). (D) The corresponding calibration curves of Fig.2C.

The impact of pH value toward the electrocatalytic performance of glucose oxidation was firstly investigated by amperometric responses. Amperometric responses of the $Ni_{0.31}Co_{0.69}S_2$/rGO modified electrode in different concentrations (0.1, 0.2, 0.3 and 0.5 M) of NaOH solution to successive additions of different concentration glucose (from 5μM to 10 mM) were shown in Fig. S4. The current responses increased with the increase of NaOH concentration from 0.1 to 0.3 mM and maintained nearly unchanged when the NaOH concentration exceeded 0.3M. Therefore, the 0.3M NaOH solution was selected as electrolyte in this work.

Fig. 3A presents the cyclic voltammetry curves (CVs) of the $Ni_{0.31}Co_{0.69}S_2$/ rGO modified electrode in 0.3 M NaOH solution in the glucose concentration from 0 to 4 mM, which is recorded at scan rate of 20mV/s. It can be seen that a pair of well-defined redox peaks located at 0.35 and 0.22V is observed in the absence of glucose, which is attributed to the redox reaction of $Ni_{0.31}Co_{0.69}S_2/Ni_{0.31}Co_{0.69}S_2OH$[41]. Upon an addition of glucose, the anodic peak current is increased and the enhancement is more obvious with the increase of glucose concentration. This phenomenon indicates the good catalytic ability of $Ni_{0.31}Co_{0.69}S_2OH$ toward glucose

($2Ni_{0.31}Co_{0.69}S_2OH + glucose \rightarrow 2Ni_{0.31}Co_{69}S_2 + gluconolactone + H_2O$). Furthermore, the insignificant redox peak shift implies the low polarization in the electrocatalytic process[42] when the glucose concentration is up to 4 mM, indicating the good reversibility of the electrode due to the little charge transfer resistance and diffusion resistance.

It should be noted that that the applied potential can strongly affect the current response of the sensor. So the applied potential was optimized through a typical I−t technique as shown in Fig.3B. When the applied potentials are increased from 0.4 to 0.5 V, the electrode delivers low background current and increased step current. But the current response is decreased accompanying with more pronounced background current when the applied potential further increased to 0.55 V. Thus, 0.5 V vs. Ag/AgCl which enables the best sensing performance for glucose oxidation was selected as the optimal applied potential in subsequent studies. Moreover, this optimal potential will have a positive effect on improving the selectivity because most of the interfering species such as uric acid (UA) and ascorbic acid (AA) are not active when the potential is below 0.5 V (vs. Ag/AgCl).[43]

The amperometric response of the $Ni_{0.31}Co_{0.69}S_2$/rGO modified electrode at 0.5 V in 0.3 M NaOH electrolyte with stepwise change of the glucose concentration is shown in Fig. 3C. It is noted that once the glucose is added to the electrolyte, the current response improved immediately and achieved 95% of the steady-state current within 3 s, indicating a fast response to glucose oxidation. As shown in Fig. 3D, the corresponding current response is linear with glucose concentration over a broad range of 0.001 to 5 mM. The sensitivity is 1753 μA mM^{-1} cm^{-2} with a correlation coefficient of 0.9965. And the detection limit is as low as 0.078 μM, calculated at a signal-to-noise ratio of 3. Moreover, in the range of 5-16 mM, the modified electrode shows another linear range with a sensitivity of 954.7 μA mM^{-1} cm^{-2} and a correlation coefficient of 0.9937. Herein, the decrease of sensitivity may be due to the adsorption of more intermediates on the surface of active materials at high concentration of glucose.[44, 45] Compared with other non-enzymatic glucose sensors previously reported (shown in Table 1), the $Ni_{0.31}Co_{0.69}S_2$/rGO modified electrode has the low detection limit, wide linear range, high sensitivity and low applied potential of 0.5 V vs. Ag/AgCl.

Table1. Comparison of the electrochemical detection performance of the $Ni_{0.31}Co_{0.69}S_2$/rGO modified electrode with other glucose sensors.

Electrode	Sensitivity (μA $mM^{-1}cm^{-2}$)	Detection limit (μM)	Linear range	Detection potential (V)	Ref.
Co_3O_4/3DGF	3390	0.025	Up to 80μM	0.58 vs. Ag/AgCl	27
$Ni(OH)_2$/3DGF	2650	0.34	1μM-1.17mM	0.55vs. Ag/AgCl	30
3D GM/NiO	918	1.6	1-100μM	0.55 vs. Ag/AgCl	29
Ni-Co NSs/RGO	1773.61	3.79	10μM-2.65mM	0.5 vs. SCE	7
Ni_3S_2/MWCNT	3345	1	30-500μM	0.54 vs. Ag/AgCl	18
$Ni_{0.31}Co_{0.69}S_2$/rGO	1753; 954.7	0.078	1μM-5mM;5-16mM	0.5 vs. Ag/AgCl	This work

3.4 Kinetic analysis of the $Ni_{0.31}Co_{0.69}S_2$/rGO modified electrode for glucose detection

Cite this: DOI: 10.1039/c0xx00000x

www.rsc.org/xxxxxx

ARTICLE TYPE

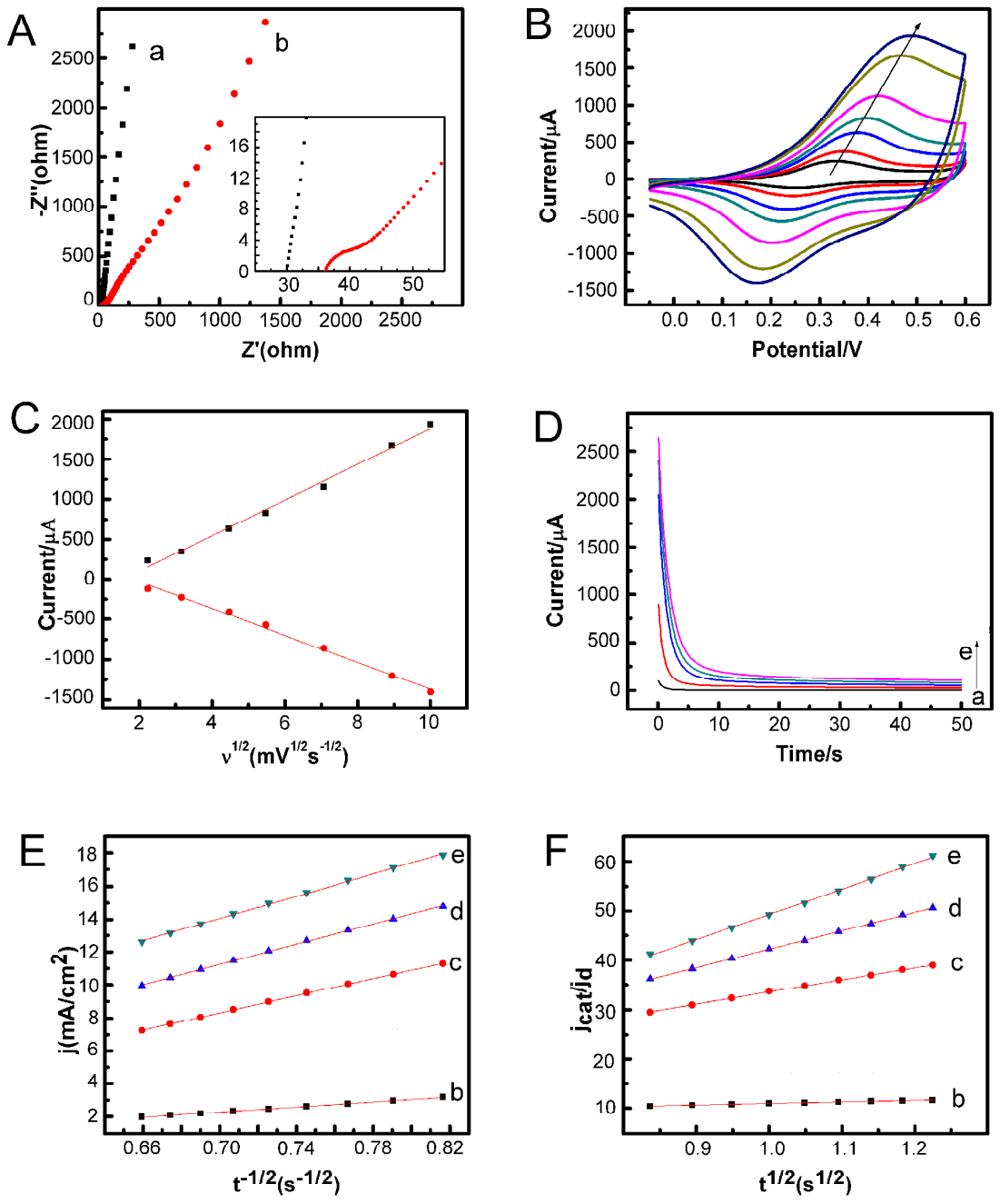

Fig.4 (A) Electrochemical impedance spectroscopy (EIS) of GCE (a) and the $Ni_{0.31}Co_{0.69}S_2$/rGO modified GCE (b) in 0.3 M NaOH solution. (B) CVs of the $Ni_{0.31}Co_{0.69}S_2$/rGO modified electrode in 0.3 M NaOH solution with 1mM glucose at various scan rates (from inner to outer curve): 5, 10, 20, 30, 50, 80, 100 mV/s. (C) The corresponding plots of anodic and cathodic peak currents vs. the square root of potential scan rate of Fig.4B. (D) Chronoamperograms of the $Ni_{0.31}Co_{0.69}S_2$/rGO modified electrode in 0.3 M NaOH solution with different concentrations of glucose: 0 mM (a), 1.0 mM (b), 2.0 mM (c), 3.0 mM (d) and 4.0 mM (e). (E) Dependency of transient current density on $t^{-1/2}$ (F) Dependency of j_{cat}/j_d on $t^{1/2}$ derived from the data of chronoamperograms curves b,c,d,e and a in Fig.4D.

Cite this: DOI: 10.1039/c0xx00000x

www.rsc.org/xxxxxx

ARTICLE TYPE

Kinetic analysis was conducted to explain the advanced electrochemical performance of the $Ni_{0.31}Co_{0.69}S_2$/rGO modified electrode by EIS, CVs and chronoamperometry response. The EIS of the $Ni_{0.31}Co_{0.69}S_2$/rGO modified electrode was measured at open circuit potential in the frequency range of 10^{-2} Hz and 10^5Hz. As shown in Fig.4A, the comparable equivalent series resistance (R_s) of the GC electrode and the $Ni_{0.31}Co_{0.69}S_2$/rGO modified electrode demonstrates the low intrinsic resistance of electroactive material. Furthermore, the small diameter of the semicircle in the high-frequency range and the nearly vertical line in the low frequency region indicate the low charge transfer resistance (R_{ct}) and diffusion resistance in the electrochemical system, demonstrating the fast reaction kinetic process. [46- 48]

Fig. 4B shows the CVs of the $Ni_{0.31}Co_{0.69}S_2$/rGO modified electrode at various scan rates of 5, 10, 20, 30, 50, 80, 100 mV/s in 0.3 M NaOH solution with the present of 1 mM glucose. In most cases, the peak separation (ΔEp) will become larger at high scan rate because a greater overpotential is needed to achieve the same rate of electron transfer. Thus, with the increase of scan rate, the small increased ΔEp value indicates the excellent reversibility of the $Ni_{0.31}Co_{0.69}S_2$/rGO modified electrode. The corresponding plots of anodic and cathodic peak currents vs. the square root of potential scan rate are shown in Fig. 4C. It can be seen that the redox peak currents are proportional to the square root of the scan rate, indicating a typical diffusion-controlled reaction.[49] Fig.4D shows the chronoamperometry response for the $Ni_{0.31}Co_{0.69}S_2$/rGO modified electrode in the absence (curve a) and presence (curve b–e: 1.0–4.0 mM) of glucose at the applied potential of 0.5 V. In a static glucose solution, a large anodic current response occurred once the potential was applied due to the oxidation of glucose. Then the current decreased gradually as the glucose near electrode surface was oxidized into gluconolactone. Finally, a stable current was maintained because of the stable concentration diffusion of glucose from bulk solution to electrode. According to the chronoamperometry curves, it can be obtained Fig. 4E and Fig.4F.[50, 51] As shown in Fig.4E, the net current vs. the minus square roots of time revealed a linear dependency. It demonstrated that the electrocatalytic oxidation of glucose was diffusion-controlled process, which is consistent with the result Fig. 4B. The diffusion coefficient (D) of glucose could be estimated as 8.54×10^{-3} cm^2 s^{-1} according to Cottrell equation:

$$j = \frac{I}{A} = nFD^{1/2}C\pi^{-1/2}t^{-1/2} \qquad (2)$$

where j is the current density (A cm^{-2}), I is the net current (A), A is the electrode surface geometrical area (cm^2), n is the electron transfer number, F is the Faraday constant (F = 96493 C mol^{-1}), C is the bulk concentration (mM) of electrolyte and t is the elapsed time (s). Besides, the time of obtained stable current depends on the catalytic rate constants (K_{cat}). Thus, from Fig. 4F, the K_{cat} can be calculated as 3.67×10^8 cm^3 mol^{-1} s^{-1} with the help of the following equation:

$$\frac{j_{cat}}{j_d} = \pi^{1/2}(K_{cat}Ct)^{1/2} \qquad (3)$$

where j_{cat} and j_d are the catalytic current density and the diffusion-controlled current density(A/cm^{-2}), respectively. C is the bulk concentration (mM) of electrolyte and t is the elapsed time (s).

As a result, the prominent electrocatalytic performance of the $Ni_{0.31}Co_{0.69}S_2$/rGO modified electrode can be attributed to the synergic effect of $Ni_{0.33}Co_{0.67}S_2$ nanoparticles and the porous graphene framework: (1) apart from the enhanced catalytic activity, the doping of Co could increase the conductivity and reduce the redox peak potentials of the $Ni_{0.31}Co_{0.69}S_2$/rGO composites; (2) the interconnected porous graphene matrix can provide buffers for electrolytes to minimize the diffusion distance of glucose to the surface of $Ni_{0.31}Co_{0.69}S_2$ which results in fast sensing response; (3) the high conductive graphene can collect electron from a vast range of reaction sites and transmit them rapidly to the electrode.

3.5. Selectivity and stability of the $Ni_{0.31}Co_{0.69}S_2$/rGO modified electrode

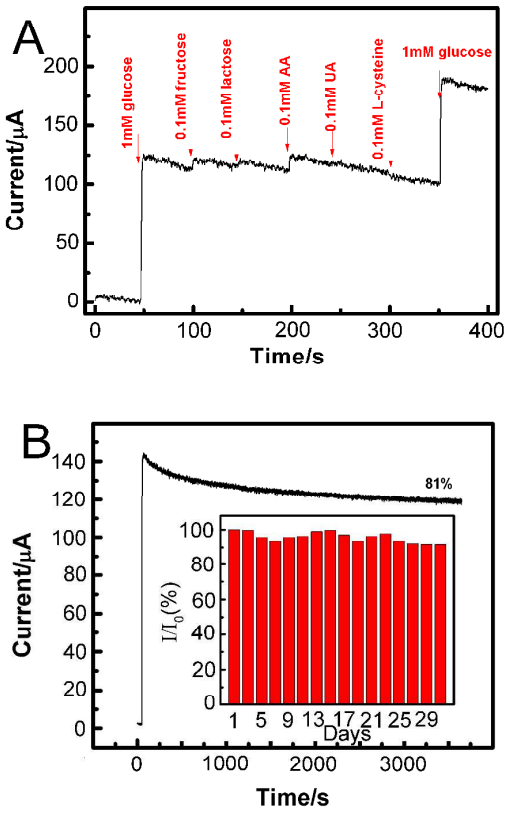

Fig. 5 (A) Amperometric response of the $Ni_{0.31}Co_{0.69}S_2$/rGO modified electrode in 0.3 M NaOH aqueous solution with successive additions of 1 mM glucose, 0.1 mM fructose, 0.1 mM lactose, 0.1 mM AA, 0.1 mM UA, 0.1 mM L-cysteine and 1 mM glucose. (B) Amperometric response towards 1 mM glucose over a long time-period of 3600 s; Inset shows the stability of the sensor to glucose tested every two days by amperometric measurement over 30 consecutive days.

Good selectivity is one of the vital characteristics of high-performance non-enzymatic glucose sensors since the interferences which have similar electroactivity usually coexist with the target analyte. In human serum, fructose, lactose, uric acid (UA) and ascorbic acid (AA) are the main interferences for the detection of glucose. But the physiological level of glucose is 3–8 mM and the levels of these interfering species are no more than 0.1 mM in normal serum.[39] Therefore, the amperometric response of the $Ni_{0.31}Co_{0.69}S_2$/rGO modified electrode with successive additions of glucose and interferences in the ratio of 10:1 was conducted. According to the results presented in Fig. 5A, the current responses produced by 0.1 mM fructose, lactose, AA, UA and L-cycteine are only 2.5%, 1.2%, 4.2%, 0.6% and 1.1% of the current response of 1 mM glucose, respectively. The excellent selectivity can be explained as follows: the porous graphene structure is beneficial to the enhanced oxidation of glucose than that of interferences due to the faster diffusion rate of glucose.[52] Furthermore, the low applied potential of 0.5V is low for the oxidation of interferences.[43, 53] In addition, the low electrocatalytic activity of the interferences (fructose and lactose) is another factor for the excellent selectivity of the modified electrode for glucose oxidation.[54, 55]

The long-term stability is important parameters to evaluate the practical application potential of the active materials. As shown in Fig. 5B, only 19% current signal is lost over a long period of 3600 s. The stability of the active materials was also tested by measuring the current response to 1 mM glucose at intervals of one day. The current response of the active materials maintains 91.6% of the initial value after one month (the inset of the Fig. 5B). These results suggest the active materials have good stability. Besides, the reusability of the electrode was determined by conducting amperometric measurements of 1.0 mM glucose for five different electrodes which prepared through the same way. The relative standard deviation (RSD) of current response is 4.55%, indicating the proposed method was reliable.

The effect of temperature for the electrocatalytic performance of the $Ni_{0.31}Co_{0.69}S_2$/rGO modified electrode was invested by amperomteric response. As shown in Fig. S5, the current responses of the $Ni_{0.31}Co_{0.69}S_2$/rGO modified electrode were increased when the temperature increased from 25 to 70℃. It is attributed to the fast redox reaction and excellent thermal stability of the as-prepared material in a high temperature.

Table 2 Concentration of glucose in human serum sample measured by commercial GOD-based glucose sensor and the as-prepared $Ni_{0.31}Co_{0.69}S_2$/rGO modified electrode

Sample	Commercial sensor (mM)	Our sensor (mM)	RSD (%) (n=3)
1	7.8	7.8	3.7
2	5.7	5.8	2.8
3	7.8	7.9	4.1

The as-prepared $Ni_{0.31}Co_{0.69}S_2$/rGO modified electrode was also used to determine the glucose concentration in human serum for practical applicability. As shown in table 2, the calculated concentration was in good agreement with the value measured by

the commercial GOD-based glucose sensor, indicating which can be utilized for the glucose detection of practical serum samples.

Conclusions

In summary, the as-prepared $Ni_{0.31}Co_{0.69}S_2$/rGO composites by hydrothermal method are composed of nearly monodisperse nanoparticles and porous reduced graphene oxide framework. Benefited from the excellent electrocatalytic activity of $Ni_{0.33}Co_{0.67}S_2$, good conductivity and high specific surface area of porous graphene framework, the $Ni_{0.31}Co_{0.69}S_2$/rGO modified electrode exhibits remarkable electrocatalytic activity towards glucose oxidation in alkaline medium, including high sensitivity, low detection limit, wide linear range and low applied potential. In addition, the $Ni_{0.31}Co_{0.69}S_2$/rGO modified electrode was confirmed to have excellent selectivity and long-term stability as well as superior practical application ability for glucose detection.

Acknowledgements

This work was supported by grants from the National Science Foundation for Fostering Talents in Basic Research of the National Natural Science Foundation of China (Grant No.J1103307), the Basic Scientific Research Business Expenses of the Central University and Open Project of Key Laboratory for Magnetism and Magnetic Materials of the Ministry of Education, Lanzhou University (LZUMMM2014001 and LZUMMM2014014), the Fundamental Research Funds for the Central University (lzujbky-2014-189), and the Science and Technology Program of Gansu Province of China (145RJZA176).

Notes and References

State Key Laboratory of Applied Organic Chemistry, Key Laboratory of Special Function Materials and Structure Design Ministry of Education, College of Chemistry and Chemical Engineering, Lanzhou University, Lanzhou 730000, China

**Corresponding author:*

Cailing Xu: Tel: +86-931-891-2589, FAX: +86-931-891-2582, Email: xucl@lzu.edu.cn

1 Heller, A.; Feldman, B., *Chemical Reviews*, 2008, **108**, 2482-2505.

2 Chen, C.; Xie, Q.; Yang, D.; Xiao, H.; Fu, Y.; Tan, Y.; Yao, S. , *RSC Advances*, 2013, **3**, 4473.

3 Si, P.; Huang, Y.; Wang, T.; Ma, J. , *RSC Advances*, 2013, **3**, 3487.

4 Lang, X.-Y.; Fu, H.-Y.; Hou, C.; Han, G.-F.; Yang, P.; Liu, Y.-B.; Jiang, Q. , *Nature Communications*, 2013, **4**.

5 Badhulika, S.; Paul, R. K.; Rajesh; Terse, T.; Mulchandani, A. , *Electroanalysis*, 2014, **26**, 103-108.

6 Senthilkumar, N.; Babu, K. J.; Gnana kumar, G.; Kim, A. R.; Yoo, D. J. , *Industrial & Engineering Chemistry Research*, 2014, **53**, 10347-10357.

7 Wang, L.; Lu, X.; Ye, Y.; Sun, L.; Song, Y. , *Electrochimica Acta*, 2013, **114**, 484-493.

8 Jiang, Y.; Yu, S.; Li, J.; Jia, L.; Wang, C. , *Carbon*, 2013, **63**, 367-375.

9 Heli, H.; Pishahang, J. , *Electrochimica Acta*, 2014, **123**, 518-526.

10 Song, J.; Xu, L.; Zhou, C.; Xing, R.; Dai, Q.; Liu, D.; Song, H. , *ACS Applied Materials & Interfaces*, 2013, **5**, 12928-12934.

11 Rui, X.; Tan, H.; Yan, Q. , *Nanoscale*, 2014, **6**, 9889-9924.

12 Pang, H.; Wei, C.; Li, X.; Li, G.; Ma, Y.; Li, S.; Chen, J.; Zhang, J. , *Scientific Reports*, 2014, **4**.

13 Cao, F.; Liu, R.; Zhou, L.; Song, S.; Lei, Y.; Shi, W.; Zhao, F.; Zhang, H. , *Journal of Materials Chemistry*, 2010, **20**, 1078.

14 Li, Z.; Gong, F.; Zhou, G.; Wang, Z.-S. , *The Journal of Physical Chemistry C*, 2013, **117**, 6561-6566.

15 Du, Y.; Yin, Z.; Zhu, J.; Huang, X.; Wu, X.-J.; Zeng, Z.; Yan, Q.; Zhang, H. , *Nature Communications*, 2012, **3**, 1177.

16 Yang, Y. J.; Zi, J.; Li, W. , *Electrochimica Acta*, 2014, **115**, 126-130.

17 Maji, S. K.; Dutta, A. K.; Bhadu, G. R.; Paul, P.; Mondal, A.; Adhikary, B. , *Journal of Materials Chemistry B*, 2013, **1**, 4127.

18 Lin, T.-W.; Liu, C.-J.; Dai, C.-S. , *Applied Catalysis B: Environmental*, 2014, **154-155**, 213-220.

19 Huo, H.; Zhao, Y.; Xu, C. , *Journal of Materials Chemistry A*, 2014, **2**, 15111-15117.

20 Guo, C.; Wang, Y.; Zhao, Y.; Xu, C. , *Analytical Methods*, 2013, **5**, 1644.

21 Lien, C.-H.; Chen, J.-C.; Hu, C.-C.; Wong, D. S.-H. , *Journal of the Taiwan Institute of Chemical Engineers*, 2014, **45**, 846-851.

22 Wolfart, F.; Lorenzen, A. L.; Nagata, N.; Vidotti, M. , *Sensors and Actuators B: Chemical*, 2013, **186**, 528-535.

23 Liu, Y.; Zhang, Y.; Wang, T.; Qin, P.; Guo, Q.; Pang, H. , *RSC Advances*, 2014, **4**, 33514-33519.

24 Chen, H.; Jiang, J.; Zhao, Y.; Zhang, L.; Guo, D.; Xia, D. , *J. Mater. Chem. A*, 2014.

25 Geim, A. K.; Novoselov, K. S. , *Nat Mater*, 2007, **6**, 183-191.

26 Wu, S.; He, Q.; Tan, C.; Wang, Y.; Zhang, H. , *Small*, 2013, **9**, 1160-1172.

27 Dong, X.-C.; Xu, H.; Wang, X.-W.; Huang, Y.-X.; Chan-Park, M. B.; Zhang, H.; Wang, L.-H.; Huang, W.; Chen, P. , *ACS Nano*, 2012, **6**, 3206-3213.

28 Yuan, M.; Liu, A.; Zhao, M.; Dong, W.; Zhao, T.; Wang, J.; Tang, W. , *Sensors and Actuators B: Chemical*, 2014, **190**, 707-714.

29 Liu, J.; Lv, W.; Wei, W.; Zhang, C.; Li, Z.; Li, B.; Kang, F.; Yang, Q.-H. , *Journal of Materials Chemistry A*, 2014, **2**, 3031-3037.

30 Zhan, B.; Liu, C.; Chen, H.; Shi, H.; Wang, L.; Chen, P.; Huang, W.; Dong, X. , *Nanoscale*, 2014, **6**, 7424.

31 Hummers, W. S.; Offeman, R. E. , *Journal of the American Chemical Society*, 1958, **80**, 1339-1339.

32 Kovtyukhova, N. I.; Ollivier, P. J.; Martin, B. R.; Mallouk, T. E.; Chizhik, S. A.; Buzaneva, E. V.; Gorchinskiy, A. D. , *Chemistry of Materials*, 1999, **11**, 771-778.

33 M. Srivastava, M. Elias Uddin, J. Singh, N. H. Kim and J. H. Lee, *Journal of Alloys and Compounds*, 2014, **590**, 266-276.

34 A. K. Das, R. K. Layek, N. H. Kim, D. Jung and J. H. Lee, *Nanoscale*, 2014, **6**, 10657-10665.

35 J. Singh, P. Khanra, T. Kuila, M. Srivastava, A. K. Das, N. H. Kim, B. J. Jung, D. Y. Kim, S. H. Lee, D. W. Lee, D.-G. Kim and J. H. Lee, *Process Biochemistry*, 2013, 48, 1724-1735.

36 K. Parvez, Z. S. Wu, R. Li, X. Liu, R. Graf, X. Feng and K. Mullen, *Journal of the American Chemical Society*, 2014, **136**, 6083-6091.

37 H.-P. Cong, X.-C. Ren, P. Wang and S.-H. Yu, *ACS Nano*, 2012, **6**, 2693-2703.

38. B. Wang, Q. Liu, J. Han, X. Zhang, J. Wang, Z. Li, H. Yan and L. Liu, *Journal of Materials Chemistry A*, 2014, **2**, 1137.

39. H. Yan, J. Bai, B. Wang, L. Yu, L. Zhao, J. Wang, Q. Liu, J. Liu and Z. Li, *Electrochimica Acta*, 2015, **154**, 9-16.

40 H. Yin, S. Zhao, J. Wan, H. Tang, L. Chang, L. He, H. Zhao, Y. Gao and Z. Tang, *Advanced materials*, 2013, **25**, 6270-6276.

41 Wang, B.; Park, J.; Su, D.; Wang, C.; Ahn, H.; Wang, G. , *Journal of Materials Chemistry*, 2012, **22**, 15750.

42 Guo, C.; Zhang, X.; Huo, H.; Xu, C.; Han, X. , *The Analyst*, 2013, **138**, 6727.

43 Guo, C.; Huo, H.; Han, X.; Xu, C.; Li, H. , *Analytical Chemistry*, 2014, **86**, 876-883.

44 El Khatib, K. M.; Abdel Hameed, R. M. , *Biosensors and Bioelectronics*, 2011, **26**, 3542-3548.

45 Wang, T.; Zhu, H.; Zhuo, J.; Zhu, Z.; Papakonstantinou, P.; Lubarsky, G.; Lin, J.; Li, M. , *Analytical Chemistry*, 2013, **85**, 10289-10295.

46 Wang, Y.-M.; Zhang, X.; Guo, C.-Y.; Zhao, Y.-Q.; Xu, C.-L.; Li, H.-L. , *Journal of Materials Chemistry A*, 2013, **1**, 13290.

47 Huo, H.; Guo, C.; Li, G.; Han, X.; Xu, C. ,*RSC Advances*, 2014, **4**, 20459.

48 J. Singh, P. Kalita, M. K. Singh and B. D. Malhotra, *Applied Physics Letters*, 2011, **98**, 123702.

49 Ji, Y.; Liu, X.; Liu, W.; Wang, Y.; Zhang, H.; Yang, M.; Wang, X.; Zhao, X.; Feng, S. , *RSC Advances*, 2014, **4**, 50220-50225.

50 Wang, L.; Zheng, Y.; Lu, X.; Li, Z.; Sun, L.; Song, Y. , *Sensors and Actuators B: Chemical*, 2014, **195**, 1-7.

51 Liu, H.; Lu, X.; Xiao, D.; Zhou, M.; Xu, D.; Sun, L.; Song, Y. , *Analytical Methods*, 2013, **5**, 6360.

52 Y. Y. Song, D. Zhang, W. Gao and X. H. Xia, *Chemistry*, 2005, **11**, 2177-2182.

53 Y. Wang, L. Luo, Y. Ding, X. Zhang, Y. Xu and X. Liu, *Journal of Electroanalytical Chemistry*, 2012, **667**, 54-58.

54 J. Jiaojiao, G. Yangyang, Z. Gangying, C. Yanping, L. Wei and H. Guohua, *Food Chemistry*, 2015, **175**, 485-493.

55 C. Guo, H. Li, X. Zhang, H. Huo and C. Xu, *Sensors and Actuators B: Chemical*, 2015, **206**, 407-414.